

Article

"Trimline Mapping from Multispectral Landsat ETM+ Imagery"

Bea M. Csatho, Cornelis J. Van Der Veen et Catherine M. Tremper

Géographie physique et Quaternaire, vol. 59, n° 1, 2005, p. 49-62.

Pour citer cet article, utiliser l'information suivante :

URI: <http://id.erudit.org/iderudit/013736ar>

DOI: 10.7202/013736ar

Note : les règles d'écriture des références bibliographiques peuvent varier selon les différents domaines du savoir.

Ce document est protégé par la loi sur le droit d'auteur. L'utilisation des services d'Érudit (y compris la reproduction) est assujettie à sa politique d'utilisation que vous pouvez consulter à l'URI <https://apropos.erudit.org/fr/usagers/politique-dutilisation/>

Érudit est un consortium interuniversitaire sans but lucratif composé de l'Université de Montréal, l'Université Laval et l'Université du Québec à Montréal. Il a pour mission la promotion et la valorisation de la recherche. Érudit offre des services d'édition numérique de documents scientifiques depuis 1998.

Pour communiquer avec les responsables d'Érudit : info@erudit.org

TRIMLINE MAPPING FROM MULTISPECTRAL LANDSAT ETM+ IMAGERY

Bea M. CSATHO*, Cornelis J. VAN DER VEEN and Catherine M. TREMPER; first and third authors: Byrd Polar Research Center, The Ohio State University, 275A Scott Hall, 1090 Carmack Road, Columbus, Ohio 43210, United States; second author: Department of Geological Sciences, The Ohio State University, 275 Mendenhall Laboratory, 125 South Oval Mall, Columbus, Ohio 43210, United States.

ABSTRACT Multispectral Landsat ETM+ imagery is used to study the ice-marginal region in the vicinity of Jakobshavn Isfjord, west Greenland. In particular, the trimline indicating margin retreat since the maximum stand attained during the Little Ice Age maximum is reconstructed, and compared with earlier maps based on aerial photogrammetry and ground surveys. Applying supervised classification, fourteen different surface types were identified, ranging from snow and ice, debris-covered ice and water with differing turbidities, to different types of vegetative landcover. After similar classes were merged into five, distinctively different classes, a digitized geomorphologic map was used to assess the accuracy of the classification. The positional accuracy of the trimline was checked by using results from a GPS survey along northern slope of the Jakobshavn fjord. By merging three spectral bands with the panchromatic band, a pan-sharpened image with a spatial resolution of 15 m is obtained that clearly shows morphological features on the ice surface, as well as increased resolution of glacial geomorphology.

RÉSUMÉ Cartographie de la limite maximale des glaces par imagerie multispectrale Landsat ETM+. La zone proglaciaire de la région de Jakobshavn Isfjord, au Groenland occidental, est étudiée par l'imagerie multispectrale Landsat ETM+, avec un accent sur la limite atteinte par les glaces durant le Petit Âge Glaciaire. L'extension maximale des glaces est reconstituée par télédétection satellitaire et comparée aux données cartographiques basées sur la photogrammétrie et des mesures de terrain. Une classification dirigée a permis d'identifier 14 types de surfaces allant de la neige et de la glace, avec ou sans débris en surface, à divers types de couverture végétale, en passant par divers degrés de turbidité de l'eau. Une carte morphologique digitale de synthèse, avec cinq classes distinctes, est produite pour déterminer la justesse de la classification. La précision de l'emplacement de la *trimline* est validée par des mesures au GPS le long du versant nord du fjord de Jakobshavn. Après la fusion de trois bandes spectrales avec la bande panchromatique, une image avec une résolution spatiale de 15 m montre clairement la morphologie des glaces, avec une finesse accrue de la géomorphologie glaciaire dans la zone marginale attenante.

INTRODUCTION

Constructing longer glacier histories, spanning the last few hundred years or so, is of particular interest for outlet glaciers draining the interior of the Greenland Ice Sheet. Repeat surveys by airborne laser altimetry in the 1990s have revealed significant thinning of the ice sheet at lower elevations (Krabill *et al.*, 2000). Specifically, some of the larger outlet glaciers are thinning at rates of several meters per year, with the most extreme thinning observed near the terminus of the Kangerlussuaq Glacier in southeastern Greenland and over the lower reaches of the Jakobshavn Glacier (Jakobshavn Isbræ) in west Greenland, with measured thinning rates as high as 10 m/yr in both locations (Thomas *et al.*, 2000, 2003). Such large thinning rates cannot be explained by a recent increase in ablation or decrease in snowfall and, instead, point to ice-dynamical processes as drivers of glacier retreat (Van der Veen, 2001; Mitchell, 2005). To fully appreciate the significance of these recent glacier changes, the magnitude of retreat and surface lowering must be placed within the broader context of retreat since the Last Glacial Maximum (LGM) and, more significantly, retreat following the temporary glacier advance during the Little Ice Age (LIA). The instrumental record of glacier observations in Greenland dates back to aerial photography conducted by the Danish Geodetic Institute in the 1930s and 1940s. Glacier histories extending farther back in time must be based on geological information retrieved from formerly glaciated regions. Depending on the age of mapped glacial-geological features, histories may be extended to the LIA and possibly as far back as the LGM, some 18 000-21 000 years ago.

The traditional approach to reconstructing paleo ice sheets from geomorphological and geological information has been to map such features during detailed field investigations. Clark (1997) noted several barriers inherent to this approach that impede synthesizing such fragmentary information into a coherent ice-sheet wide picture. In most cases there are few links between spatially separate studies, or there are large gaps in spatial coverage. Moreover, in many instances, control on dating is poor, thus casting doubt on the commonly-made assumption that similar features reported in different studies are coeval. These difficulties can be partially overcome through the use of remote sensing, which allows for greater spatial coverage of geological features (Clark, 1997).

As he has noted, "A major problem in validating ice sheet models is that geologically-based information has been derived mostly from fieldwork and usually relates to only small sectors of ice sheets which can be thought of as point evidence. Furthermore there are frequently unresolved contradictions between local areas. A methodology that attempts to provide information on wider spatial scales and promote greater analysis and coherence of all evidence is by use of remote sensing and ... GIS".

Early geological applications of remote sensing were based on high-resolution aerial photogrammetry. According to Clark (1997), the study of Sugden (1978) was the first to demonstrate the usefulness of satellite images to provide glacial-geomorphological information over large areas. In that study, a Landsat MSS photomosaic was used to produce a proxy map of the intensity of glacial erosion by the Laurentide Ice

Sheet. Subsequent applications have included mapping of depositional landforms (Punkari, 1982), identification and mapping of previously unrecognized mega-lineaments (Clark, 1993; Clark *et al.*, 2000), and mapping margins of paleo ice streams (Stokes and Clark, 2002). A review of earlier work is provided by Clark (1997). The objective of the present study is to explore the feasibility of using multispectral Landsat ETM+ images to map trimlines in the coastal regions of Greenland.

In mountainous regions, former higher stands of glaciers that retreated recently (since the Little Ice Age maximum) are frequently marked by trimlines on the walls of valleys and fjords previously occupied by these glaciers (Fig. 1). Erosional action of the moving ice causes vegetation to be removed where the ice is in contact with the surrounding rock walls. The upper limit of this eroded region, which becomes exposed as the glacier retreats and its surface is lowered, is called the trimline (Flint, 1971: p. 144). Mapping of trimlines and other glacio-geomorphological features thus allows reconstruction of the neoglacial history of glaciers.

Historical evidence indicates that in many parts of the Greenland Ice Sheet the major historical maximum occurred almost simultaneously during the last decades of the 19th century (Weidick, 1984). Therefore, mapping of the trimline zone over larger areas and possibly the entire ice sheet could provide an estimate of the total area deglaciated as well as the total ice volume lost since then. Indeed, based on comparison between trimline elevations and the current ice-surface elevation in west Greenland, Weidick (1968) estimated an average loss of 200 km³/year ice from the whole Greenland Ice Sheet since the Little Ice Age, corresponding to an average rise of 0.6 mm/year in global sea level. This is equivalent to a 30 800 km³ total loss or 90 mm global sea level rise since 1850.

The ability to map surficial features from satellite imagery depends on obtaining spectral signatures of these features that are markedly different from the signatures of surrounding regions. With respect to trimlines, spectral reflectance

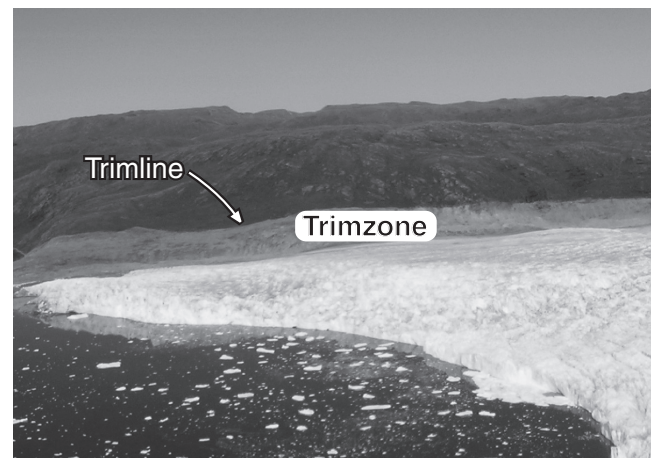


FIGURE 1. Trimline zone on a steep slope, north of Sermeq Avannarleq, West Greenland (see Fig. 2 for location).

Limite des glaces sur une pente abrupte, au nord de Sermeq Avannarleq, Groenland occidentale (voir fig. 2 pour la localisation).

differences may be associated with variations in vegetative cover above and below the trimline. The LIA trimlines are usually characterized by sharp vegetation boundaries. Outside the trimzone, flat and gentle slopes are often covered by tundra vegetation, while steeper rock surfaces are lichen-covered. Inside trimline regions, rock surfaces are fresh and bare, retaining their original color and spectral properties (Knight *et al.*, 1987). It is well known that vegetation can easily be mapped using visible and near infrared (NIR) spectral imagery. Several studies have demonstrated the pronounced effect of lichens on the reflectance spectrum of the land surface (Satterwhite *et al.*, 1985; Ager and Milton, 1987; Rivard and Arvidson, 1992; Bechtel *et al.*, 2002; Van der Veen and Csatho, this issue). Thus, spectral property information from multispectral satellite images can be used to locate the boundary between vegetation-covered and vegetation-free surfaces. This boundary is the trimline.

CHARACTERISTICS OF LICHENS

Lichens are “an association of a fungus and a photosynthetic symbiont resulting in a stable thallus of specific structure” (Hawksworth and Hill, 1984). Lichens occur in most habitats around the world and communities are usually classified according to their substrate. Worldwide, approximately 13 500 taxa of lichenized fungi are recognized (Hawksworth and Hill, 1984). Lichens, which do not have special organs or structures for water storage, shut down metabolically when dry, allowing them to withstand longer periods of dryness. Because of this opportunistic usage of available moisture, lichens can survive in environments that are low or deficient in moisture available for the support of plant life. In these so-called xeric environments, lichens spend much of the time in a dry, inactive state (Lawrey, 1984).

Rock substrates provide stable habitats for the establishment of long-term lichen communities. On these surfaces, lichens grow at relatively uniform rates of time scales of centuries or millenia. Once attached to a substrate, lichens do not move during their lifespan and thus the age of lichens can be considered a proxy for the minimum exposure time of the substrate to the atmosphere and sunlight. These two characteristics form the basis for lichenometry, a biological technique for estimating the age of exposed and stabilized rock surfaces (Locke *et al.*, 1979). In short, the assumption is made that the size of the largest individual thallus on a substrate is a function of the time the substrate has been exposed. Using surfaces of known exposure age, a lichenometric dating curve can be established that relates surface exposure age to the largest lichen size. This dating curve is then applied to estimate the exposure age of other surfaces based on the largest size of lichens found on these surfaces (Noller and Locke, 2000). Lichenometry has been applied in glacial geology and geomorphology at many sites around the world including dating the LIA maximum in Iceland (Kirkbridge and Dugmore, 2001), in South America (Winchester and Harrison, 2000) and in Alaska (Haworth *et al.*, 1986). Beschel, who is regarded as the “Father of lichenometry”, has pioneered lichenometric dating in west Greenland (Beschel, 1961).

While the study presented here focuses on determining the spatial extent of lichen-covered rocks, exploratory

lichenometry was conducted and a tentative dating curve for dating glacio-geomorphological features exposed since the LIA was derived. Results of that part of our study will be discussed in a forthcoming paper.

The spectral characteristics of lichens are discussed more fully in Bechtel *et al.* (2002) and in a companion paper (Van der Veen and Csatho, this issue), but some details are worth repeating here. Spectra of lichens in the 400-700 nm range vary primarily with pigmentation, and in the 700-1 350 nm range reflectance increases steadily and remains high or only slightly decreasing at greater wavelengths, in contrast to the reflectance of green, leafy plants, which tends to rise almost vertically from the visible to the near-infrared and decreases slowly from 800-1 300 nm (Ager and Milton, 1987). Absorption bands centered at 1 450, 1 935 and 2600 nm are attributed to water in lichens. Since these water absorption features are usually weaker than in vascular plants, they do not mask the effect of cellulose, which causes broad absorption bands at 1 730, 2 100 and 2 300 nm (Bechtel *et al.*, 2002).

To our knowledge, the only previous study of spectral properties of lichens and lichen-covered rock from Greenland was published by Rivard and Arvidson (1992). The authors collected *in situ* spectra of different surfaces, including lichen-covered rocks, on Qilangarsuit Island on the west coast to investigate whether Landsat Thematic Mapper (Landsat TM) multispectral imagery can be used for lithologic mapping in Arctic regions. They concluded that Landsat TM data can be used as first order products to distinguish between tundra vegetation that typically covers older moraines at lower elevations, and lichen-covered bedrock exposed at higher elevations. Mapping of different lithologies with Landsat TM imagery is severely hampered by the limited spectral and radiometric capabilities of the sensor as well as by the ubiquitous lichen cover. For the purpose of mapping trimlines, however, requirements are less stringent and the results of Rivard and Arvidson (1992) are encouraging as these indicate the possibility of distinguishing between tundra cover, lichen-covered rocks, and bare rock surfaces.

PREVIOUS TRIMLINE STUDIES

It has long been recognized that trimlines can be mapped using aerial photography. For example, Weidick (1992; reproduced in Fig. 7: right panel) presents glacial erosion trimzones along the margins of Jakobshavn Isbræ in west Greenland, mapped from stereo aerial photographs acquired in 1985. However, as noted by Clark (1997), aerial photographs, while capable of providing excellent high-resolution information on geomorphological features, typically cover limited areas and extending this procedure to cover regions formerly occupied by entire ice sheets is a daunting task. Because of the greater area captured by a single image (typically 60 by 60 km or larger), satellite imagery permits greater areas to be studied efficiently. To our knowledge, the study of Knight *et al.* (1987) is thus far the only study to use satellite images to map trimlines and ice-sheet retreat.

Landsat Multispectral Scanner (MSS) imagery, acquired in July 1982, was used by Knight *et al.* (1987) to identify recently deglaciated regions bordering the present-day ice sheet margin

in the vicinity of Jakobshavn Isbræ. In the MSS-5 band (red, 600-700 nm), a light-tinged zone fringing the ice sheet and extending down both flanks of Jakobshavn Isfjord was noted. The outer limit of this zone appeared to be marked by a sharp boundary in vegetation cover. Using supervised classification of all four MSS bands, Knight *et al.* (1987) distinguished six different classes of surface types, namely sediment filled lakes, clear lakes, ice cap, glacier debris, vegetated area, and poorly vegetated areas within the trimline. Feature space boundaries of the classes for the parallelepiped classification were defined by the standard deviation of the spectral values in the training sets. The good separability of the classes in feature space indicated that sufficient spectral contrast exists between fresh rock surfaces, and vegetation and lichen-covered rocks. In particular, poorly vegetated areas within the trimline were isolated from regions covered with shrub tundra and lichen cover, primarily through their higher reflectance in bands MSS-4 (green, 500-600 nm) and MSS-5 (red, 600-700 nm). Since the spectral contrast along the trimline depends on the type of vegetation, rocks and moraines exposed within the trimzone (Satterwhite *et al.*, 1985; Ager and Milton, 1987; Van der Veen and Csatho, this issue) the four bands of the Landsat MSS sensor allow detection of trimlines only for certain combinations of lichen and rock reflectance. Therefore, the procedure followed by Knight *et al.* (1987) may not be directly applicable to other sites. The more recent Landsat TM and Enhanced Thematic Mapper (ETM+) systems have six spectral bands within a wider spectral range (450 to 2 350 nm) enabling a better discrimination between different landcover types and therefore these sensors are more suitable for mapping trimlines. Moreover, the Landsat TM and ETM+ systems have higher spatial resolution, namely 30 m Instantaneous Field Of View (IFOV) of the multispectral bands and 15 m IFOV of panchromatic band (ETM+ only) compared with the 79 m IFOV of the Landsat MSS, enabling mapping of smaller geomorphological features, such as small moraines.

FEASIBILITY STUDY: JAKOBSHAVN ISBRÆ

The drainage basin of Jakobshavn Isbræ (known also as Sermeq Kujalleq), named after the nearby town of Jakobshavn (Ilulissat) on the west coast of Greenland (Fig. 2), is one of the most dynamically active parts of the Greenland Ice Sheet. The calving terminus of this glacier receded 25 km between 1850 and 1950 from the head of the fjord to the position shown on the Landsat image used in this study (Weidick, 1992: Fig. 2; reproduced in Fig. 7). Fresh moraines and trimlines exposed on the fjord walls suggest a lowering of the glacier surface by up to 250-300 m since the LIA maximum (Weidick, 1992). Recent results indicate further retreat (Podlech and Weidick, 2004), widespread thinning over the lower part of the drainage basin (Thomas *et al.*, 2003) and substantial increase in velocity (Joughin *et al.*, 2004). Because of these ongoing changes, as well as the availability of prior studies in this region (Thomsen, 1983; Thomsen, 1986; Knight *et al.*, 1987; Thomsen and Winding, 1988; Thomsen *et al.*, 1988; Weidick, 1992; Prescott, 1995; Hughes, 1998; Sohn *et al.*, 1998), this area was selected for the feasibility study.

The Landsat ETM+ imagery, taken on July 7, 2001, covers Jakobshavn Isfjord and a 200 km long stretch of the ice sheet

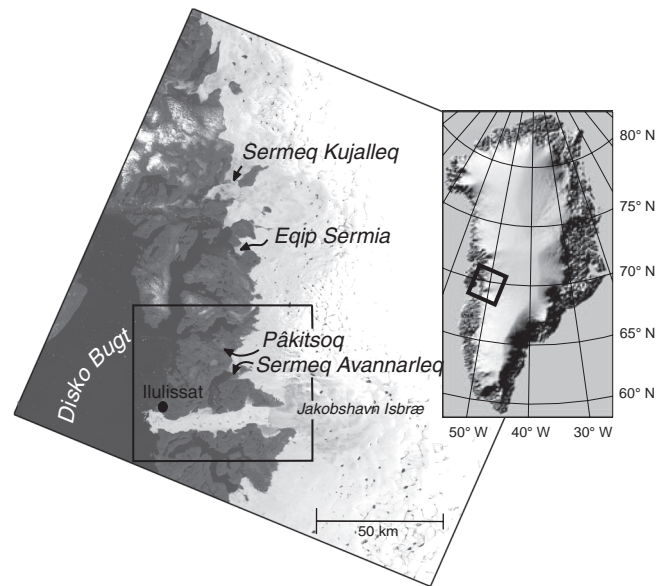


FIGURE 2. Location of the study site (highlighted area) on July 7, 2001, Landsat ETM+ scene, WRS-2, Path 009, Row 011, orthorectified. Source for this dataset was the Global Land Cover Facility (<http://www.landcover.org>). The inset shows the location of Landsat scene on a shaded relief topographic map of Greenland.

Localisation du site d'étude (encadré) à partir d'une image Landsat ETM+ prise le 7 juillet 2001, WRS 2, trajectoire 009, rangée 011, orthorectifiée. La base de données provient du Global Land Cover Facility (<http://www.landcover.org>). L'insertion montre l'emplacement de l'image Landsat sur une carte topographique du Groenland.

margin north of the fjord (Fig. 2). The boxed area around the fjord, measuring approximately 65 km by 75 km, was selected for this pilot study because of the availability of detailed land cover information. In addition to image analysis described in this paper, exploratory fieldwork was conducted around Ilulissat and in and around the field camps marked in Figure 3. The major objectives of the field campaign were to collect the spectra of various land surfaces and vegetation types and to map glacio-geological features, including trimline locations. Van der Veen and Csatho (this issue) summarizes the results of the spectral measurements. Results from the spectral measurements and from the glacial geologic mapping were also used in this study, for example for training site selection and for assessing the accuracy of the classification. The study site is depicted in Figure 3 as a false color composite of Landsat ETM+ bands 2, 3 and 4. This "color infrared" image shows vegetation in different hues of red, while water, snow, and ice surfaces are depicted in blue, ranging from the dark blue over sea water to white over snow covered regions. Exposed rock surfaces and man-made objects are characterized by grayish-brownish hues. At the time of the image acquisition, most of the seasonal snow cover had melted from the coastal mountains, exposing the rock and vegetation surfaces.

The land area is hilly upland, composed of rounded knolls of crystalline bedrock with elevation ranging from sea level to ~650 m. The bedrock consists of Precambrian crystalline rocks, mostly gneiss, with amphibolite dykes in the immediate study

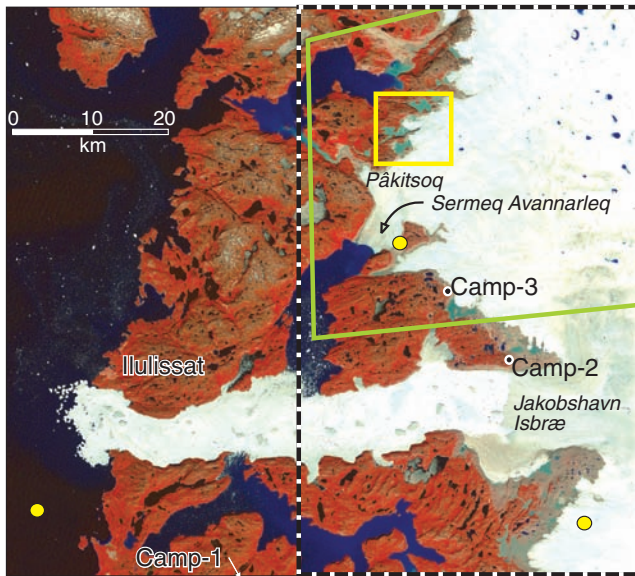


FIGURE 3. False color composite image of study site from Landsat bands 2 (blue), 3 (green) and 4 (red). Reddish color indicates vegetation, snow and ice have different tones of blue and white, and exposed rock surfaces and sediments have greyish-brownish hues. Green box marks area covered by the Thomsen and Winding (1988) glacial geomorphological map, dashed box marks region enlarged in Figure 7 and yellow boxed area is enlarged in Figure 9. Camps were occupied in the 2003 field season. Yellow circles mark regions where water, exposed rocks and firn pixels were selected for establishing the Empirical Line Correction (EML) conversion.

Image fausse couleur du site d'étude à partir des bandes 2 (bleu), 3 (vert) et 4 (rouge). Les couleurs rouges indiquent la végétation, la neige et la glace sont illustrées en différents tons de bleu et de blanc, les surfaces rocheuses et les sédiments possèdent des teintes grises et brunes. Le rectangle vert délimite la zone couverte par la carte géomorphologique glaciaire de Thomsen et Winding (1979), le rectangle en noir pointillé délimite la région agrandie à la figure 7 et le rectangle jaune est l'agrandissement de la figure 9. Les camps sont occupés pendant la campagne de terrain de 2003. Les cercles jaunes marquent les régions de pixels d'eau, de roches exposées et de névé qui ont servi à la conversion de la Ligne de Correction Empirique.

region (Geological Survey of Denmark and Greenland, 1997). The area, typical of west Greenland, is characterized by a landscape of glacial scouring (Sugden, 1974). The satellite image depicts the landforms of glacial erosion (Fig. 3), irregular depressions having been produced along joints, faults and dykes, some of which are occupied by lakes in the deeper basins.

Over the exposed land the predominant reflectance feature is the high NIR reflectance (reddish color of the IR composite) indicating that the surface is covered by a patchwork of vegetation and lichens. The vegetation is of low-arctic type with predominant plant communities of heath (moor), fell-field, herb-slope, willow-scrub, fen, river- and seashore vegetation. Mikkelsen and Ingerslev (2002) include details on these plant communities as well as a comprehensive plant list of the Ilulissat area. The most abundant lichens are dark grey to black crustose and foliose ephelitic (rock-growing) lichen (Van der Veen and Csatho, this issue). The brownish-grayish band between the ice sheet and the land corresponds to fresh rock surfaces exposed by retreat of the ice sheet since the LIA. Similar light-

colored bands are observed around some of the lakes, where the former higher water level destroyed the lichen cover.

The clear water in fjords bordering Disko Bay (Disko Bugt), and supraglacial lakes are shown in dark blue. Most of the lakes in the ice free terrain also have dark blue colors. Lakes close to the ice sheet margin have lighter blue shades indicating higher reflectance in the visible and in the NIR, probably caused by fine-grained, suspended sediment, originating from englacial and subglacial channels and glacier melt-streams. Fresh snow covering the higher elevation parts of the land and ice sheet surface is white. Older snow, firn and glacier ice appear in different shades of blue. The image also depicts the details of the ice sheet surface morphology, including crevasse zones, meltwater streams, and debris cover adjacent to the margin. Jakobshavn Isfjord is filled with brash ice surrounding a few icebergs and bergy bits. Some of the lakes on the surrounding land are still covered by ice.

ANALYSIS OF LANDSAT IMAGERY

PREPROCESSING

Orthorectification

The orthorectified Landsat ETM+ scene, taken on July 7, 2001 (Fig. 2), was obtained free of charge from the Global Land Cover Facility (<http://www.landcover.org>). The sun elevation angle was 42 degrees and the sun azimuth was 169 degrees during the image acquisition. Landsat images of Greenland in this global data set were registered by using manually selected control points in a block-adjustment involving all scenes covering Greenland, followed by orthorectification using the 30-arc-second GTOPO30 (1 km) Digital Elevation Model (Tucker *et al.*, 2004). The estimated planimetric accuracy of the orthorectified images is better than 50 m Root Mean Square Error (RMSE).

Atmospheric correction

We applied the Empirical Line Correction (EML) model to convert the raw Digital Number (DN) values of the six multi-spectral bands into surface reflectance. The EML technique uses a band-to-band linear regression between the pixel samples and reference reflectance spectra to establish the transformation from the DNs to surface reflectance (Kruse *et al.*, 1990). Because of the remoteness of sufficiently large homogeneous regions, we could not collect field spectra suitable for establishing this transformation. Therefore we followed the normal practice of using laboratory spectra as reference spectra (Rosenthal and Dozier, 1996) by selecting water, snow and gneiss laboratory spectra from the Johns Hopkins University Spectral Library (included in Environment for Visualizing Images, ENVI 4.1, from Research Systems, Inc.). Corresponding regions of the Landsat imagery are marked in Figure 3. Water pixels were extracted over open sea water. For snow, we selected an area of darker, possibly melting, snow to avoid saturation of the visible bands over bright, fresh snow. These snow pixels, taken near the ice margin, SE of Jakobshavn fjord, were paired with the spectra of coarse, granular snow from the spectral library. Landsat pixels over outcropping rocks, south of Sermeq

Avannarleq, and felsitic gneiss reference spectra were chosen for representing the typical granodioritic to quartz dioritic gneiss rocks of the region (Geological Survey of Denmark and Greenland, 1997). To assess the performance of the EML conversion we compared the reflectance values derived from Landsat imagery with spectra measured by using a Fieldspec[®] PRO spectrometer from Analytical Spectral Devices, Inc. over the runway of the Ilulissat airport during our 2003 field campaign. The good agreement between the reflectance values [$\text{reflectance}_{\text{Landsat}} = (0.089, 0.117, 0.123, 0.145, 0.190, 0.194)$ and $\text{reflectance}_{\text{field}} = (0.110, 0.125, 0.129, 0.139, 0.175, 0.185)$, vector components refer to Landsat spectral bands] confirms the accuracy of the EML reflectance conversion.

Topographic correction

A Digital Elevation Model (DEM) of the site, generated from stereo Advanced Spaceborne Thermal Emission and Reflection Radiometer (ASTER) by using the ASTERDTM ENVI module from Sulsoft, Brazil, was used for topographic correction. Stereo aerial photographs and GPS observations, both from the National Survey and Cadastre, Denmark, provided control information for the generation of the DEM. The application of a simple topographic correction procedure based on the cosine law (Bishop and Shroder, 2004) caused overcorrection over steep slopes. This effect is especially pronounced over slopes with cast shadows facing away from the sun. This problem occurs because the cosine correction does not account for secondary illumination, such as diffuse skylight and light reflected from adjacent terrain. Since the use of the topographic correction did not increase the classification accuracy, as was demonstrated by several test runs over small sites, we decided to use the uncorrected reflectance images.

SURFACE CLASSIFICATION

Before the supervised classification of the non-thermal Landsat bands, we examined their spectral information content by using unsupervised classification and different visualization tools (e.g. scatterplots and n-dimensional visualizer) provided by the ENVI software. We identified 14 different spectral classes, related to different snow, ice and water conditions, and different vegetation, rock and sediment types (Table I). Training sites are well distributed within the study area shown in Figure 3. When selecting the training sites we relied on the following data sources: (1) topographic maps (National Survey and Cadastre of Denmark, 2000); (2) geomorphologic maps (Thomsen and Winding, 1988); (3) geologic maps (Geologic Survey of Greenland, 1974; Geologic Survey of Denmark and Greenland, 1997); (4) stereo aerial photographs acquired in 1985 (National Survey and Cadastre of Denmark, 2000; 1 : 150 000 scale); (5) historical photographs, for example in Mikkelsen and Ingerslev (2002) and in Weidick (1968); (6) field observations conducted around the town of Ilulissat, around Camps 1-3 and in the Pâkitsoq area in 2003 (Fig. 3).

Separability of classes was checked during the selection process by computing the transformed divergence of the training sets (Schowengerdt, 1997). Transformed divergence measures the separability of samples by considering both their

TABLE I

Major spectral and information classes of the study site

| Class labels | Spectral class | Land surface category |
|--------------|--|-----------------------|
| A | Ice, snow and firn | a: Ice |
| B | Melting ice, snow and firn | |
| C | Supraglacial lakes and brash ice | |
| D | Clear water | b: Water |
| E | Slightly turbid water | |
| F | Moderately turbid water | |
| G | Turbid water | |
| H | Lichen-dominated vegetation | c: Land |
| I | Tundra-dominated vegetation | |
| J | Wet glaciofluvial and eolian sediments | |
| K | Glaciofluvial and eolian sediments | |
| L | Debris-covered ice | d: Debris-covered ice |
| M | Trimline zone, no vegetation | e: Trimzone |
| N | Trimline zone, some vegetation | |

means and covariance matrices. If the transformed divergence of classes was less than the threshold of good separability (1.9), the training sets were modified. A total of ~108 200 training pixels in 59 training areas (~2% of the pixels in the classified scene) were selected to establish the statistics of the 14 landcover classes.

The classification map, presented in the upper panel of Figure 4, was obtained by Maximum Likelihood (ML) classification of the six non-thermal multispectral bands of the Landsat ETM+ imagery. The classified image was filtered by using a 3 by 3 majority filter (weight of central pixel = 3), to remove isolated pixels. To delineate the trimline zones, the spectral classes were combined into five information classes in the lower panel of Figure 4: (a) ice, snow, firn and supraglacial lakes; (b) water (from clear to turbid); (c) land, including vegetation-covered surfaces and glaciofluvial and eolian deposits; (d) debris-covered ice and (e) trimzones.

The average spectra of the 14 different surface classes are depicted in Figure 5. Although the low spectral resolution of the Landsat sensor and the effect of spectral mixing somewhat complicate the interpretation of these spectra, most land cover type exhibits well-known spectral shapes and absorption features.

Freshly fallen snow has a very high reflectance in the visible wavelength and the reflectance rapidly decreases toward the NIR and MIR (spectrum A). Spectrum B, observed mostly over upland lakes and in fjords, has a shape similar to spectrum A, but the reflectance is lower throughout the whole spectral range. Reflectance of fresh snow, firn, and ice is reduced by the presence of impurities, debris cover and surface meltwater (Hall and Martinec, 1985), and we interpret class B as melting ice or pieces of floating, calving ice in fjords. The shape of spectrum C, which includes pixels measured over supraglacial lakes, is quite different. The high reflectance at blue and green (bands 1-2) indicates that the energy at shorter wavelengths penetrates

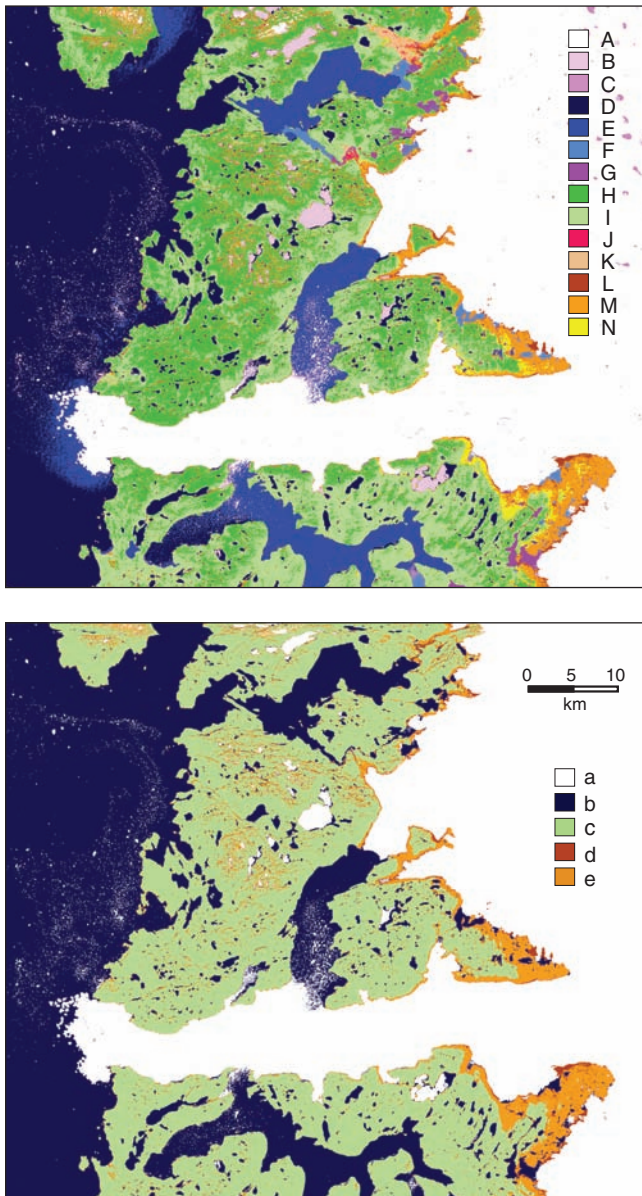


FIGURE 4. (Upper panel) Result of maximum likelihood supervised classification. (Lower panel) Surface categories obtained by merging spectral classes as shown in Table I.

(Haut) Résultat de la classification dirigée selon la méthode du maximum de ressemblance. (Bas) Catégories de surfaces obtenues par la synthèse des classes spectrales telles que définies au tableau I.

deep enough to be reflected from the bottom ice. However, as the penetration depth in water decreases with increasing wavelength, the reflectance is rapidly decreasing and the spectrum becomes similar to water spectra.

Open, clear water (spectrum D) has a low overall reflectance. Multiple scattering, caused by suspended silt in the water, increases the reflectance in the visible and NIR wavelengths observed in spectra E, F and G, with increasingly higher reflectance indicating progressively more turbidity (Mertes *et al.*, 2004: p. 374). The ability to distinguish changes in turbidity

could permit monitoring sediment load in proglacial lakes, streams and fjords from multispectral satellite imagery. Since most suspended sediments originate from englacial and subglacial channels and glacier melt-streams, this, in turn, could provide important information about glacial and subglacial hydrologic systems.

Spectra of biogenic surfaces (spectra H, I and N) show typical spectral signatures of lichens (the reflectance maximum in the MIR band) and vascular vegetation (sudden increase of reflectance in NIR, also called "red edge"). Class I shows a more pronounced red edge, with a smaller maximum in band 5, suggesting that this class has more tundra vegetation and less lichen-covered rock than class H. To explain the spectral signatures of these classes, we computed the spectral curves of mixed pixels from field spectra of typical land cover types, collected around Camp-2 during the 2003 field season (see Van der Veen and Csatho (this issue) for details in data acquisition). The upper left panel of Figure 6 shows the field spectra of (1) *Slip arctica* (Arctic willow) that represents vascular vegetation; (2) *Umbilicaria cylindrica*, a black, foliose lichen, covering large parts of rock outcrops above the trimline and (3) light-colored gneiss, which is a significant constituent of the exposed soils and sediments. The spectral library resampling tool of ENVI 4.1 was used to resample these field spectra into the spectral resolution of the Landsat ETM+ sensor, resulting in the spectra presented in the upper right panel. We computed the spectra of mixed pixels, shown in the lower panel (thin lines), by assuming linear mixing of the different components. By comparing these spectra with the average spectra of vegetation-covered areas from the Landsat ML classification (shown by thick lines), we estimate that class H (lichen-dominated vegetation) has 70% lichen and 20% vascular vegetation cover, while class I (tundra and lichen vegetation) has only slightly more lichen-covered area (50%) than vascular vegetation (40%). The percentage of outcrop is 10% for all modeled cases. Our results demonstrate that Landsat TM and ETM+ data can be used as first order products to distinguish between tundra vegetation that typically covers older moraines at lower elevations (class I), and lichen-covered bedrock exposed at higher elevations (class H). We should emphasize that determining the distribution of different land cover types within mixed pixels is an ill-posed problem and therefore the result of spectral unmixing is somewhat influenced by the end-member selection.

The spectra of exposed sediments and rocks (spectra J, K and M) have very similar shapes with no major absorption features. Class K, characterized by a reflectance increasing with wavelength in the visible and near constant, high reflectance in the NIR/MIR domains indicates the presence of fine grained material, with low organic matter content and with no or minimum vegetation cover. This class is found in outwash plains and fluvial terraces deposited from braided rivers and according to the Quaternary geologic map it corresponds to eolian and glaciofluvial sediments. The spectrum of class J has a similar shape but an overall lower reflectance with a pronounced decrease in reflectance toward the end of the spectrum, indicating similar material but higher moisture content. Therefore class J is interpreted as wet glaciofluvial and eolian sediments. The featureless spectral curve of M is

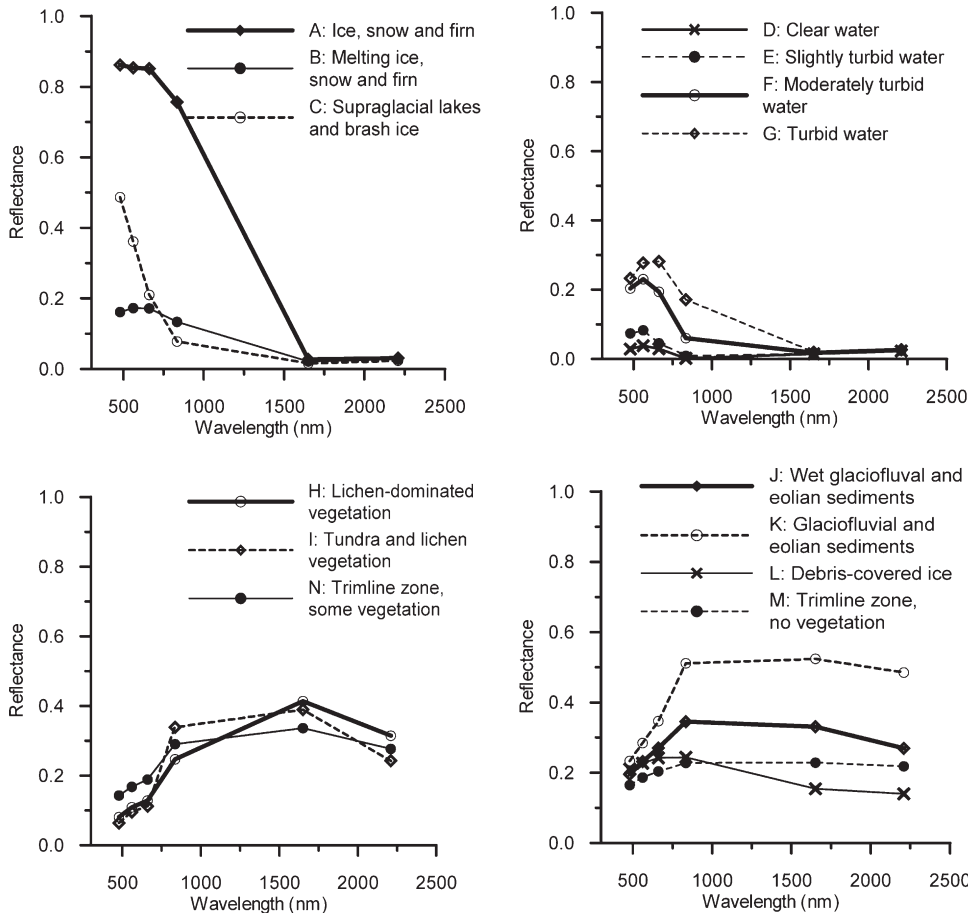


FIGURE 5. Mean spectra of classes obtained by maximum likelihood classification.

Classes spectrales moyennes obtenues à partir de la classification dirigée selon la méthode du maximum de ressemblance.

typical for the moraines and outcrops of the trimline zones. Finally, the spectrum of class L is similar to the spectra of moraines and the trimline zone (class M) in the visible and NIR domains, but has slightly lower reflectance in the MIR domain. This surface type is restricted to narrow zones on the ice sheet located next to the ice sheet margin and corresponds to debris-covered ice.

VERIFICATION OF GLACIAL GEOMORPHOLOGICAL MAPPING, ACCURACY ASSESSMENT

Pixel-based accuracy assessment

The glacier-hydrological map of Thomsen and Winding (1988), chosen to assess the accuracy of the classification, covers the northeastern part of the area (green polygon in Fig. 3). This 1 : 75 000 scale photogrammetric map is based on aerial photographs acquired on July 10, 1985. To facilitate the pixel-based comparison, the hardcopy map was scanned and re-projected to the same coordinate system as the Landsat image. The main purpose of the map was to depict glacial geomorphological features, therefore features on the land area were generalized. For example, small patches of exposed rock and many small lakes and streams, clearly visible on the Landsat image, are absent in the published map. Trimline zones were only marked along the ice sheet and

outlet glaciers, but not in the large valleys, formerly occupied by glacier tongues or outlet glaciers. We used information from historical photographs (Wedick, 1968; Mikkelsen and Ingerslev, 2002) to estimate the extent of the trimline zone in these valleys (Fig. 7).

Since the map did not distinguish between different vegetation types and water conditions, we could only perform a rigorous accuracy assessment on the classification map with the combined classes (Fig. 4: lower panel). Additionally, we combined the (d) debris-covered ice and (e) trimline zone classes because (1) the boundary between these classes was not mapped accurately in large areas (marked as "inferred" on the map), and (2) changes in the ice sheet boundary between the time of acquisition of the aerial photographs and the Landsat imagery were most significant in areas where a wide band of debris covered the ice sheet margin in the published map.

Four hundred random points, 100 points per class, were chosen from the map using a stratified random selection procedure (Richards and Jia, 1999: p. 267). To reduce the effect of the generalized nature of the map and the coregistration errors, a window size of 5 by 5 was used in the selection of the points, and a threshold value of 18 (out of 25) was stipulated before a point was eligible for selection. Points retained for the accuracy assessment were distributed among the classes as

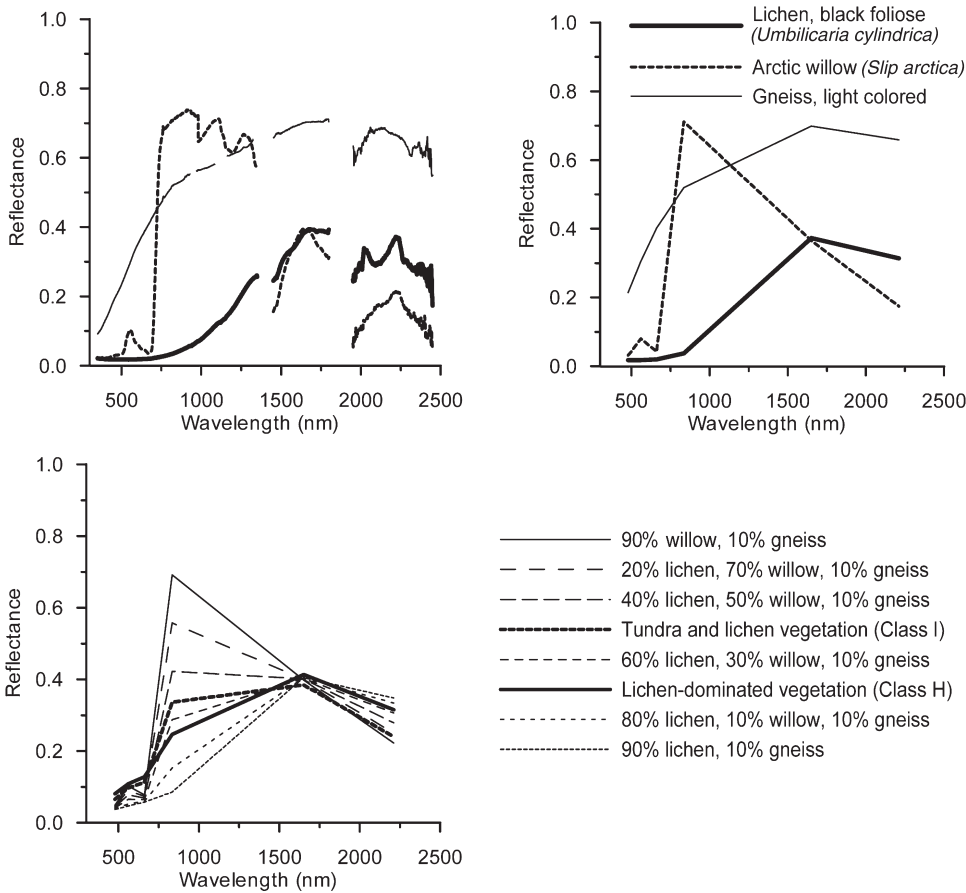


FIGURE 6. Spectral curves of typical tundra surfaces. (Upper left panel) Field spectra of vascular vegetation (Arctic willow, *Slip arctica*), black foliose lichen (*Umbilicaria cylindrica*) and light-colored gneiss, measured by Fieldspec® PRO spectrometer from Analytical Spectral Devices, Inc. (Upper right panel) Same spectra resampled into resolution of Landsat ETM+ sensor. (Lower panel) Effect of linear spectral mixing. Thin lines show spectra of mixed pixels of lichen, arctic willow and gneiss with different ratios and thick lines are mean spectra of Tundra and lichen vegetation (class I) and Lichen dominated vegetation (class H) from maximum likelihood classification of Landsat imagery.

Courbes spectrales des surfaces typiques de toundra. (Haut, gauche) Spectres de végétation vasculaire (saule pourpre nain, Slip arctica), de lichen (Umbilicaria cylindrica) et de gneiss faiblement teinté, mesurés avec un spectromètre Fieldspec® PRO de Analytical Spectral Devices, Inc. (Haut, droite) Courbes spectrales ré-échantillonnées à la résolution du capteur Landsat ETM+. (Bas) Effet du mélange linéaire des spectres. Les lignes fines montrent les spectres résultant du mélange des pixels de lichen, de saule pourpre nain et de gneiss à divers ratios et les lignes épaisses représentent les spectres moyens de la végétation de toundra et de lichen (classe I) et de la végétation dominée par le lichen (classe H) à partir de la classification selon la méthode du maximum de ressemblance pour l'imagerie Landsat.

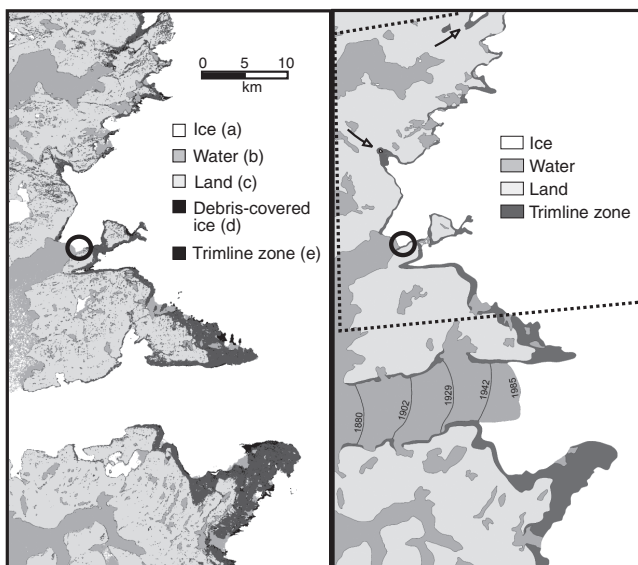


FIGURE 7. Accuracy assessment. (Left panel) Major surface categories from maximum likelihood classification around Jakobshavn Isbræ (same categories as in Fig. 4). (Right panel) Map of erosional trimline zone and recession of calving front from Weidick (1992) and Thomsen and Winding (1988). Extent of trimline zones in formerly glaciated valleys are estimated from historical photographs (Weidick, 1968; Mikkelsen and Ingerslev, 2002). Circle in both panels shows a typical location of trimline zone pixels misclassified as water due to cast shadows from steep slopes. Arrows in the right panel indicate valleys where information from historical photographs was used to estimate the extent of the trimline zone.

Validation de la classification. (Gauche) Principales catégories de surface issues de la classification dirigée selon la méthode du maximum de ressemblance pour la région de Jakobshavn Isbræ (mêmes catégories qu'à la fig. 4). (Droite) Carte des zones d'érosion en bordure des glaces et retrait du front glaciaire d'après Weidick (1992) et Thomsen et Winding (1988). L'extension maximale des glaces dans les vallées glaciaires a été estimée à partir de photographies historiques (Weidick, 1968; Mikkelsen and Ingerslev, 2002). Les cercles sur les deux côtés montrent une zone typique de limite des glaces qui a été incluse dans la catégorie eau à cause de l'ombrage produite par les pentes abruptes.

follows: ice, 98 points; water, 94 points; land, 81 points and trimline zone and debris on ice, 56 points.

Table II shows the error matrix from the accuracy assessment, the accuracy totals and the Kappa-statistics. The overall classification accuracy of 93.3% with an overall Kappa statistics of 0.9105 is very good. Discrepancies between the classified pixels and the reference data were potentially caused by actual retreat of the ice sheet margin (ice/snow/firn class replaced by trimline zone or debris on ice class) or by the presence of large barren (non-vegetated) areas over the ice-free land, mostly around lakes or along streams (land pixels which were classified as trimline zones or debris on ice).

Checking completeness and accuracy of trimline zone mapped from Landsat imagery

In addition to the pixel-based accuracy assessment using the Thomsen and Winding (1988) map, we also evaluated the accuracy and completeness of trimline zone (classes M and N in the upper panel and class e in the lower panel of Fig. 4, also depicted as the dark grey zone in the left panel of Fig. 7) around the ice sheet over a larger area. The ground truth map, shown in the right panel of Figure 7, is compiled from the map of Thomsen and Winding (1988) in the north and a map from Weidick (1992) in the south. Weidick's map is based on the Geological Survey of Greenland topographic map sheet (1 : 250 000), which was drawn on the basis of point determinations and aerial photographs. The trimline zone obtained by the classification of Landsat imagery (dark grey) agrees very well with the trimline zone mapped by traditional methods. Errors include the exclusion of trimline zone pixels (error of omission) on steep slopes that cast shadows, causing trimline zone pixels to be classified as water (Fig. 7: circled region located south of Sermeq Avannarleq). Inclusion of non-trimline

zone pixels into the trimline zone class (error of commission) is observed in large valleys (*i.e.* Pâkitsoq), where some glaciofluvial sediments are classified as trimline zone. Some bare patches along rivers or around lakes or in upland areas are also classified as trimline zone.

Figure 8 shows the location of the trimline, as measured by a handheld GPS receiver during the 2003 field campaign. The planimetric accuracy of the GPS measurements was about 10 m RMSE. The average distance between the trimline locations derived from the Landsat imagery and the corresponding GPS measurements is less than the Landsat pixel size (28.5 m), demonstrating the geometric and thematic accuracy of the classified Landsat image. Red dots in Figure 8 show the boundary between regions with some vegetation and with absolutely no vegetation within the trimzone. These measurements and the fact that the boundary between the non-vegetated (class M, orange) and somewhat vegetated trimzones (class N, yellow) is nearly parallel with the inferred boundary of the paleo ice sheet, suggest that classes M and N mark trimline zone surfaces which have been exposed for different lengths of time.

Pansharpening of Landsat imagery for glacial geomorphological mapping

The detailed map of Thomsen and Winding (1988) also provides physiographic information, including features related to surface hydrology of the ice sheet. Mapped features include supraglacial lakes and streams, moulins, crevasses, as well as lineaments influencing the drainage pattern. Part of this map, covering the area north of Pâkitsoq (indicated by a yellow box in Fig. 3), is shown in Figure 9, together with a Landsat ETM+ based satellite image-map and the supervised classification map. The satellite image-map is a pan-sharpened false color

TABLE II

Class accuracy assessment report

| Classification | Reference data | | | | Total |
|--------------------------------|----------------|-------|------|-------------------------|-------|
| | Ice/snow/firn | Water | Land | Trimzone, debris on ice | |
| a: Ice/snow/firn | 94 | 2 | 0 | 2 | 98 |
| b: Water | 0 | 89 | 3 | 0 | 92 |
| c: Land | 0 | 1 | 72 | 0 | 73 |
| d + e: Trimzone, debris on ice | 6 | 2 | 6 | 54 | 68 |
| Total | 100 | 94 | 81 | 56 | 331 |

| Classification | Producer's accuracy | User's accuracy |
|--------------------------------|---------------------|-----------------|
| a: Ice/snow/firn | 94.0% | 95.9% |
| b: Water | 94.7% | 96.7% |
| c: Land | 88.9% | 98.6% |
| d + e: Trimzone, debris on ice | 96.4% | 79.4% |

Overall classification accuracy = 93.3%

Overall Kappa statistics = 0.9105

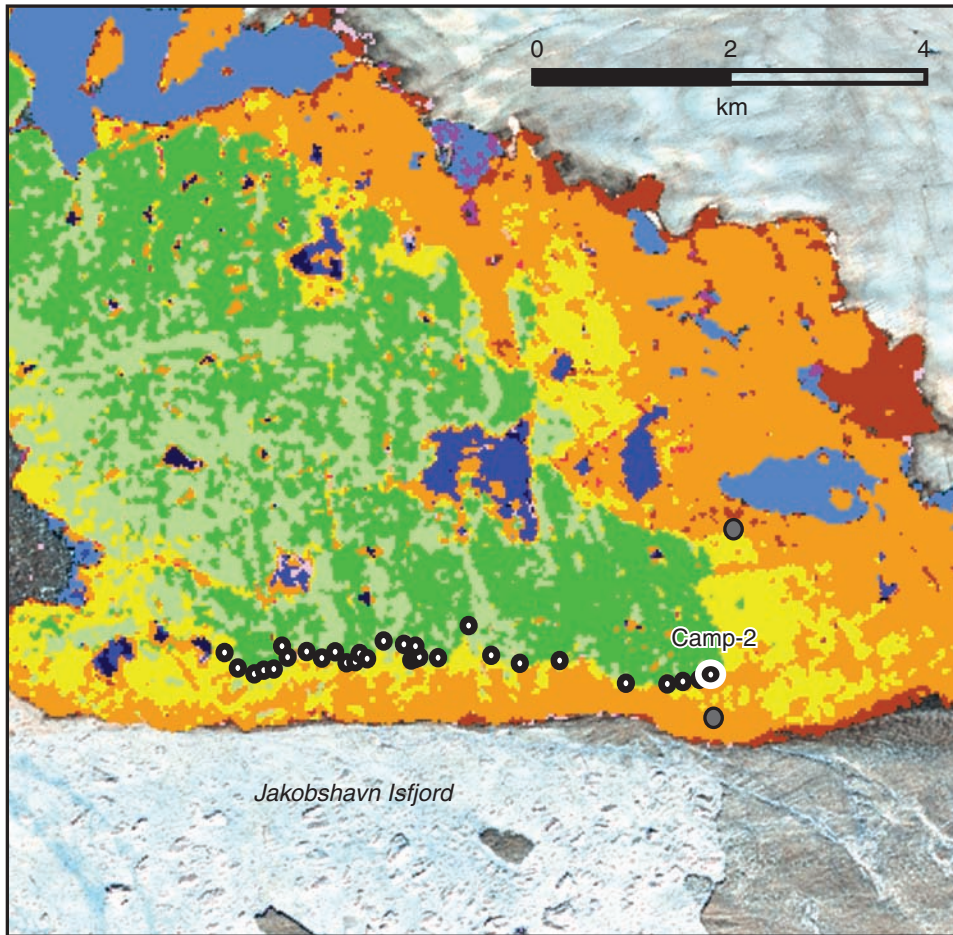


FIGURE 8. Verification of trimline location extracted from maximum likelihood classification results (colors) by using ground GPS measurements of trimlines around Camp-2. Black circles show trimline positions measured by GPS and red circles mark the boundary between bare rocks and partially lichen and vegetation covered surfaces.

Vérification de l'emplacement de la limite maximale des glaces entre les résultats de la classification dirigée selon la méthode du maximum de ressemblance (couleurs) et des points de mesure GPS sur le terrain autour du Camp-2. Les cercles noirs montrent l'emplacement des points GPS de la limite maximale des glaces et les cercles rouges indiquent la bordure entre les roches nues et les surfaces recouvertes partiellement par des lichens et de la végétation.

composite of bands 2, 3 and 4. A special image fusion technique, the Boverly transform (Gupta, 2003: p. 268), was used to merge three multispectral bands with the higher spatial resolution panchromatic band. The fused image has the spatial resolution of the panchromatic band, while preserving the spectral information of the multispectral bands. The satellite image map is a very rich source of geometric information. It shows many details of the physiography of the ice sheet surface such as crevasse fields, supraglacial lakes, and flow traces that can be used to infer drainage patterns. On the adjacent land, the image shows glacial geomorphological features. This information can be combined with the classification map which distinguishes surfaces based on composition or nature of the land cover (e.g. debris-covered ice, fresh snow, etc.). Together, this provides a more comprehensive picture of the landscape than can be obtained from the pan-sharpened image or the classification map alone.

DISCUSSION

The primary motivation for the present study is the need to place recent changes observed on Greenland outlet glaciers in the broader context of glacier changes since the LIA maximum, *i.e.* 1850. Recognizing the limitations inherent to traditional field-based geological approaches, a multispectral

Landsat ETM+ scene was analyzed to map trimline zones in the vicinity of Jakobshavn Isbræ, west Greenland. By utilizing information contained in the six non-thermal spectral bands, imaged surfaces can be classified according to their spectral reflectance characteristics. As demonstrated in Figure 4 (upper panel), this classification encompasses more than the distinction between bare rock and vegetation cover that defines the trimline. Indeed, different snow and ice facies, as well as water bodies with different turbidity are distinguished, and distribution of glaciofluvial and fluvial sediments and trimline sub-zones is mapped.

As our accuracy assessment confirms, we can reliably distinguish between vegetation-covered areas and trimline zones. It is well known that vascular vegetation has a very strong spectral contrast in the NIR. As several recent studies demonstrated (Bechtel *et al.*, 2002; Van der Veen and Csatho, this issue) the shape of the reflectance spectra for lichens is very different from that of other surface types or landcovers as well. Notably, the NIR maximum, around 1 600 nm, is a unique feature of the lichen spectra. Since vascular vegetation is also characterized by distinct spectral signatures we believe that trimlines can be mapped reliably over different rock types using images that cover the broad spectral range up to 2 400 nm. As such, the techniques applied in this study present an advantage over trimline mapping from aerial photographs, which may be

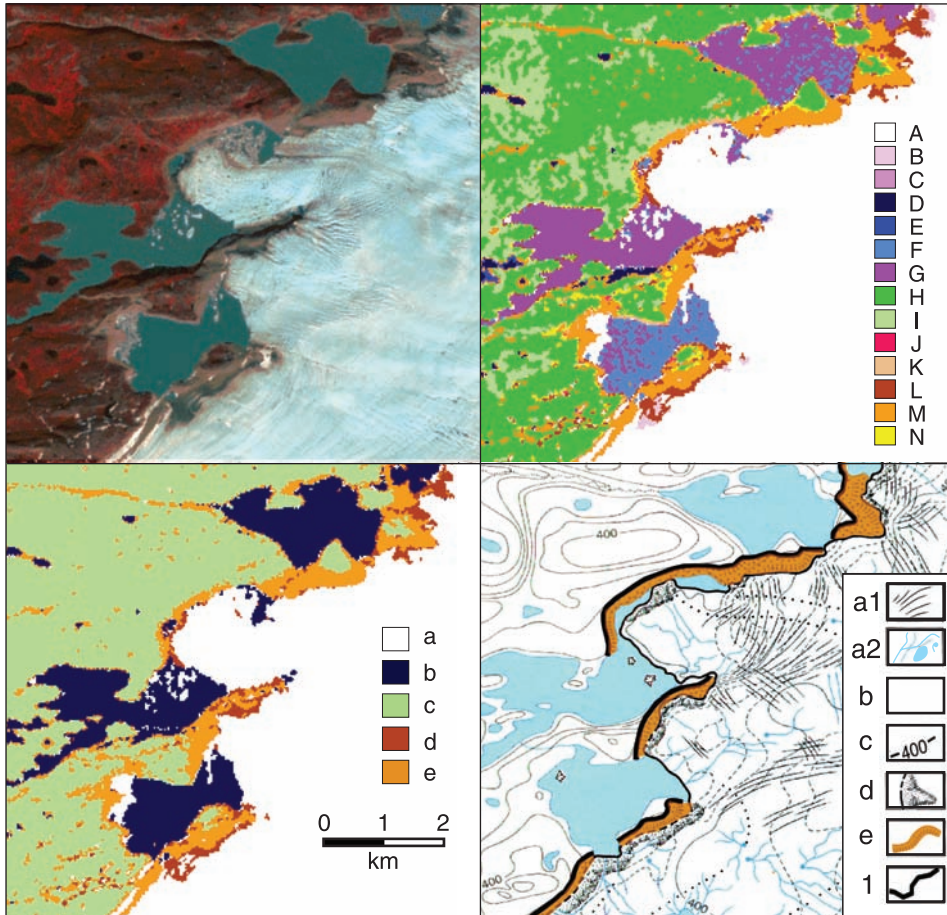


FIGURE 9. Mapping glacial geomorphology and drainage from Landsat ETM+ imagery. (Upper left panel) Pan-sharpened color composite of Landsat bands 2, 3 and 4, and 15 metres resolution panchromatic band. (Upper right panel) Classified Landsat ETM+ scene, see Figure 4 (upper panel) for land-cover classes. (Lower left panel) Major surface categories after merging the 14 spectral classes into 5 major landcover classes. (Lower right panel) Details of geomorphologic map of Thomsen and Winding (1988): (a) ice surface features including (a1) crevasses and lineations and (a2) streams, moulins and supraglacial lakes; (b) water in lakes and fjords; (c) land with surface elevation contours; (d) debris-covered ice and (e) trimline zone with (1) trimline.

Cartographie de la géomorphologie glaciaire et du réseau de drainage à partir de l'imagerie Landsat ETM+. (Haut, gauche) Image composée des bandes 2, 3, et 4 et de la bande panchromatique à 15 m de résolution. (Haut, droite) Image multispectrale Landsat ETM+ classifiée, voir la figure 4 pour la légende des classes. (Bas, gauche) Principales catégories de surface suite au regroupement des 14 classes spectrales en cinq classes. (Bas, droite) Détails de la carte géomorphologique de Thomson et Winding (1988) : (a) glace en surface incluant (a1) des crevasses et des linéaments et (a2) des cours d'eau, des moulins et des lacs supraglaciaires; (b) eau de lacs et de fjords; (c) courbes de niveau; (d) glace recouverte de débris et (e) zones de la limite maximale des glaces.

efficient where the bedrock consists primarily of gneiss, but which may not work very well in the case of dark, basaltic bedrock (Weidick, 1968).

In most cases, the trimline zone and debris-covered ice can be distinguished, but there may be problematic areas, depending on the distribution of surface material. The spectrum of debris-covered ice is a mixture of the spectrum of debris material and that of ice. Clearly, in places where the ice is fully covered with debris the boundary between debris-covered ice and ice-free morainal plains can not be detected by spectral analysis only. However, even relatively small patches of exposed ice reduce the reflectance in longer wavelengths.

In this study, supervised surface classification was used in which training samples of different cover types are selected by the operator. This is a feasible approach when considering small regions, as was done here, and it allowed assessing the usefulness of multispectral imagery for trimline mapping without the need for designing more automated techniques. For larger projects, however, automation of trimline mapping is

not only possible but also desirable. Such automation can be achieved for example by using a multi-dimensional edge detector algorithm to find simultaneous changes in all or most spectral bands. This procedure would extract all boundaries, not only the transition between exposed rock and lichen and vegetation cover. Thus, to obtain the actual trimline, additional constraints are needed, possibly based on a geometric-topological model. For instance, defining the trimline zone as a narrow band bordering the ice margin, candidate boundaries for the trimline can be selected from the entire ensemble of boundaries. It should be noted, however, that in all likelihood the final selection will require some input from the operator.

Mapping trimlines provides information on the spatial extent of ice margin retreat. While horizontal changes can be determined reliably from Landsat imagery, obtaining a fully three-dimensional reconstruction requires additional information. Accurate determination of the elevations of trimlines is essential for estimating loss in ice volume. Printed maps are available for the region but their accuracy is insufficient for use as

reference DEM. A better approach would be to use stereo pairs of aerial photographs to extract ground control points and to measure a DEM of the study region. Using these ground control points and the DEM, the Landsat image and the aerial photographs can be precisely co-registered and the elevation of the trimline be directly measured from the stereo photographs. An alternative solution is to use ASTER imagery. The ASTER sensor simultaneously provides multispectral imagery and stereo coverage for measuring surface elevations, allowing the user to measure the location and elevation of the trimline from the same data set. Moreover, fusion of spectral information with surface elevation provided promising results for mapping debris-covered glaciers (Paul *et al.*, 2004), a problem very similar to the detection of the boundary between the trimline zone and debris-covered ice. We are currently in the process of conducting a pilot study for mapping trimline zone around the Jakosbhavns Isfjord from a combined data set of Landsat imagery and aerial photographs and from ASTER imagery.

In addition to mapping different types of surfaces based on their spectral properties, Landsat imagery can also be used for morphologic mapping of the ice surface, in particular features such as flow lines, surface lakes and streams, and crevasse zones. By merging three multispectral bands with the higher spatial resolution panchromatic band, the spatial resolution increases from 30 m to 15 m for the pan-sharpened image. This dramatically improves the ability to identify morphological features than can be used to describe and constrain the spatial pattern of ice flow and drainage.

In summary, the pilot study presented here has demonstrated that glacier trimlines can be mapped with confidence from multispectral Landsat images. The key to success is the wide spectral range of Landsat, from 400 to 2 400 nm. The procedures are sufficiently expedient to allow for mapping trimlines around the entire perimeter of the Greenland Ice Sheet. Doing so would provide a benchmark for its maximum extent during the LIA. Comparison of this benchmark with the present-day ice sheet would provide more quantitative estimates of changes in ice volume over the past ~150 years, and hence of the contribution of the Greenland Ice Sheet to global sea level since the Industrial Revolution. This would allow the estimated current contribution to be placed in a broader context and provide better understanding of the behavior of the ice sheet and its interaction with climate.

ACKNOWLEDGEMENTS

This study was supported through grants from NASA (NAG5-13614) and the National Science Foundation (NSF-OPP-9911981). We thank Valery Gataullin, for GPS measurements of trimline locations, Yushin Ahn, BPRC, for assistance in preparing the illustrations and Toni Schenk, OSU, for valuable advices about automatic detection of trimline zones. Referee comments on an earlier version of this manuscript helped to improve the clarity and presentation of this material. This is Byrd Polar Research Center Contribution number C-1289.

REFERENCES

Ager, C.M., and Milton, N.M., 1987. Spectral reflectance of lichens and their effects on the reflectance of rock substrates. *Geophysics*, 52: 898-906.

- Bechtel, R., Rivard, B. and Sánchez-Azofeifa, A., 2002. Spectral properties of foliose and crustose lichens based on laboratory experiments. *Remote Sensing of Environment*, 92: 389-396.
- Beschel, R.E., 1961. Dating rock surfaces by lichen growth and its application to glaciology and physiography (lichenometry), p. 1044-1062. *In* G.O. Raasch, ed., *Geology of the Arctic*, Vol.2. University of Toronto Press, Toronto, 1196 p.
- Bishop, M.P. and J.F. Shroder, 2004. *Geographic Information Science and Mountain Geomorphology*. Praxis Publishing, Chichester, 486 p.
- Clark, C.D., 1993. Mega-scale glacial lineations and cross-cutting ice-flow landforms. *Earth Surface Processes and Landforms*, 18: 1-29.
- Clark, C.D., 1997. Reconstructing the evolutionary dynamics of former ice sheets using multi-temporal evidence, remote sensing and GIS. *Quaternary Science Reviews*, 16: 1067-1092.
- Clark, C.D., Knight, J.K. and Gray, J.T., 2000. Geomorphological reconstruction of the Labrador Sector of the Laurentide ice sheet. *Quaternary Science Reviews*, 19: 1343-1366.
- Flint, R.F., 1971. *Glacial and Quaternary Geology*. John Wiley and Sons, New York, 892 p.
- Geologic Survey of Greenland, 1974. 1 : 500 000 Quaternary Geologic Quadrangle Maps, Sheet 3, Søndre Strømfjord-Nūgssuaq.
- Geological Survey of Denmark and Greenland, 1997. 1 : 500 000 Geological Map of Greenland, Sheet 3, Søndre Strømfjord-Nūgssuaq, compilation by Escher in 1971. *Geology of Denmark and Greenland Map Series*, Copenhagen, Denmark, CD-ROM.
- Gupta, R.P., 2003. *Remote Sensing Geology*. Springer-Verlag, Berlin, 655 p.
- Hall, D.K. and Martinec, J., 1985. *Remote sensing of ice and snow*. Chapman and Hall, New York, 189 p.
- Hawksworth, D.L., and Hill, D.J., 1984. *The lichen-forming fungi*. Blackie, London, 158 p.
- Haworth, L.A., Calkin, P.E., and Ellis, J.M., 1986. Direct measurements of lichen growth in the central Brooks Range, Alaska, USA, and its application to lichenometric dating. *Arctic and Alpine Research*, 18: 289-296.
- Hughes, T.J., 1998. *Ice Sheets*. Oxford University Press, New York, 343 p.
- Joughin, I., Abdalati, W. and Fahnestock, M., 2004. Large fluctuations in speed on Greenland's Jakobshavn Isbræ glacier. *Nature*, 432: 608-610.
- Kirkbridge, M.P. and Dugmore, A.J., 2001. Can lichenometry be used to date the "Little Ice Age" glacial maximum in Iceland? *Climatic Change*, 48: 151-167.
- Knight, P., Weaver, R. and Sugden, D.E., 1987. Using Landsat MSS data for measuring ice sheet retreat. *International Journal of Remote Sensing*, 8: 1069-1074.
- Krabill, W., Abdalati, W., Frederick, E., Manizade, S., Martin, C., Sonntag, J., Swift, R., Thomas, R., Wright, W. and Yungel, J., 2000. Greenland ice sheet: High-elevation balance and peripheral thinning. *Science*, 289: 428-429.
- Kruse, F.A., Kierein-Young, K.S. and Boardman, J.W., 1990. Mineral mapping at Cuprite, Nevada with a 63-channel imaging spectrometer. *Photogrammetric Engineering and Remote Sensing*, 56: 83-92.
- Lawrey, J.D., 1984. *Biology of lichenized fungi*. Praeger Publishers, Westport, 408 p.
- Locke, W.W., Andrews, J.T. and Webber, P.J., 1979. A manual for lichenometry. *British Geomorphological Group, Technical Bulletin* 28, 47 p.
- Mertes, L.A.K., Dekker, A.G., Brakenridge, G.R., Birkett, C.M. and Létourneau, G., 2004. Rivers and lakes, p. 345-400. *In* S. Usting, ed., *Remote Sensing for Natural Resources Management and Environmental Monitoring, Manual of Remote Sensing*, Vol. 4, John Wiley and Sons, Hoboken, 736 p.
- Mikkelsen, N. and Ingerslev, T., eds., 2002. Nomination of the Ilulissat Icefjord for inclusion in the World Heritage list. *Geological Survey of Denmark and Greenland (GEUS)*, Copenhagen, 136 p.
- Mitchell, J.B., 2005. Increased thinning at Kangerlussuaq Glacier, southeastern Greenland: climate variability and its potential impact on glacier dynamics. M.Sc. thesis, The Ohio State University, 120 p.
- National Survey and Cadastre of Denmark, 2000. *Greenland Topographical Atlas*, CD-ROM.

- Noller, J.S., and Locke, W.W., 2000. Lichenometry, p. 261-272. *In* J.S. Noller, J.M. Sowers and W.R. Lettis, eds., *Quaternary Geochronology*. American Geophysical Union, AGU Reference Shelf 4.
- Paul, F., Huggel, C. and Käb, A., 2004. Combining satellite multispectral image data and a digital elevation model for mapping debris-covered glaciers. *Remote Sensing of Environment*, 89: 510-518.
- Podlech, S. and Weidick, A., 2004. A catastrophic break-up of the front of Jakobshavn Isbræ, West Greenland. *Journal of Glaciology*, 50: 153-154.
- Prescott, P., 1995. Photogrammetric examination of the calving dynamics of Jakobshavn Isbræ, Greenland. Ph.D. thesis, University of Maine, 107 p.
- Punkari, M., 1982. Glacial geomorphology and dynamics in the eastern parts of the Baltic Shield interpreted using Landsat imagery. *Photogrammetric Journal of Finland*, 9: 77-93.
- Richard, J.A., and Jia, X., 1999. *Remote Sensing Digital Image Analysis, an Introduction*. Springer-Verlag, Berlin, 363 p.
- Rivard, B., and Arvidson, R.E., 1992. Utility of imaging spectrometry for lithologic mapping in Greenland. *Photogrammetric Engineering and Remote Sensing*, 58: 945-949.
- Satterwhite, M.B., Henley, J.P. and Carney, J.M., 1985. Effects of lichens on the reflectance spectra of granitic rock surfaces. *Remote Sensing of Environment*, 18: 105-112.
- Schowengerdt, R.A., 1997. *Remote sensing models and methods for image processing*. Academic Press, San Diego, 522 p.
- Sohn, H.G., Jezek, K.C. and Van der Veen, C.J. 1998. Jakobshavn Glacier, West Greenland: 30 years of spaceborne observations. *Geophysical Research Letters*, 25: 2699-2702.
- Stokes, C.R., and Clark, C.D., 2002. Ice stream shear margin moraines. *Earth Surface Processes and Landforms*, 27: 547-558.
- Sugden, D.E., 1974. Landscapes of glacial erosion in Greenland and their relationship to ice, topographic and bedrock conditions, p. 177-195. *In* E.H. Brown and R.S. Waters, eds., *Progress in geomorphology*. Institute of British Geography, Special publication 7.
- Sugden, D.E., 1978. Glacial erosion by the Laurentide ice sheet. *Journal of Glaciology*, 20: 367-391.
- Thomas, R.H., Abdalati, W., Akins, T., Csatho, B., Frederick, E., Gogineni, P., Krabill, W., Manizade, S. and Rignot, E., 2000. Substantial thinning of a major east Greenland outlet glacier. *Geophysical Research Letters*, 27: 291-294.
- Thomas, R.H., Abdalati, W., Frederick, E., Krabill, W.B., Manizade, S. and Steffen, K., 2003. Investigation of surface melting and dynamic thinning on Jakobshavn Isbræ. *Journal of Glaciology*, 165: 231-239.
- Thomsen, H.H., 1983. Glaciologiske undersøgelser ved Pâkitsup ilordlia 1982, Ilulissat/Jakobshavn. Grønlands Geologiske Undersøgelse, Gletcher-hydrologiske Meddelelser 83/3, 24 p.
- Thomsen, H.H., 1986. Photogrammetric and satellite mapping of the margin of the Inland Ice, West Greenland. *Annals of Glaciology*, 8: 164-167.
- Thomsen, H.H. and Winding, O., 1988. Margin of the Inland Ice north-east of Jakobshavn (Paakitsup Akuliarusersua 1985) glacier hydrological map, 1 : 75 000. The Geological Survey of Greenland.
- Thomsen, H.H., Thorning, L. and Braithwaite, R.J., 1988. Glacier-hydrological conditions on the inland ice north-east of Jakobshavn/Ilulissat, West Greenland. Grønlands Geologiske Undersøgelse Rapport, 138, 1 sheet.
- Tucker, C.J., Grant, D.M. and Dykstra, J.D., 2004. NASA's global orthorectified Landsat data set. *Photogrammetric Engineering and Remote Sensing*, 70: 313-322.
- Van der Veen, C.J., 2001. Greenland ice sheet response to external forcing. *Journal of Geophysical Research*, 106: 34047-34058.
- Van der Veen, C.J. and Csatho, B., 2005. Spectral characteristics of Greenland lichens. *Géographie physique et Quaternaire*, 59: 63-73.
- Weidick, A., 1968. Observations on some Holocene glacier fluctuations in West Greenland. Grønlands Geologiske Undersøgelse Bulletin, No. 73, 202 p.
- Weidick, A., 1984. Studies of glacier behaviour and glacier mass balance in Greenland – a review. *Geografiska Annaler*, 66A: 183-195.
- Weidick, A., 1992. Jakobshavn Isbræ area during the climatic optimum. Rapport Grønlands Geologiske Undersøgelse, 155: 67-72.
- Winchester, V. and Harrison, S., 2000. Dendrochronology and lichenometry: colonization, growth rates and dating of geomorphological events on the east side of the North Patagonian Icefield, Chile. *Geomorphology*, 34: 181-194.